Charged particle of mass m and velocity $\vec{\beta}c$ interacts electromagnetically with detector medium via a photon of energy $\hbar\omega$ and momentum $\hbar\vec{k}$

Basics
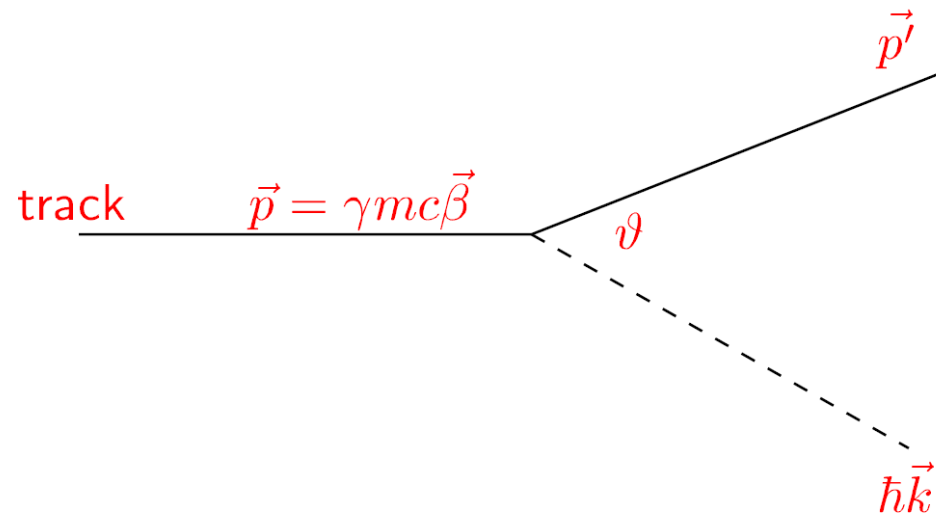
Conservation of energy and momentum gives

$$\hbar\omega(1 - \frac{\hbar\omega}{2\gamma mc^2}) = \hbar\vec{k} \cdot \vec{\beta}c - \frac{\hbar^2 k^2}{2\gamma m}$$

typically $\hbar\omega << \gamma mc^2$ and $\hbar k << \gamma mc \rightarrow$

$$\omega = \vec{k} \cdot \vec{\beta}c = \beta ck \cos\vartheta. \tag{1}$$

Basics: dE/dx, Čerenkov, Trans. Rad - 2

The photon also has to satisfy the dispersion relation for a given medium with a dielectric constant ϵ

$$\omega^2 - \frac{k^2 c^2}{\epsilon} = 0 \tag{2}$$

From (1) and (2) we get

$$\sqrt{\epsilon}\beta \cos \vartheta = 1$$

which has a solution with a real value of ϑ if

$$\sqrt{\epsilon}\beta = n\beta > 1. \tag{3}$$

In this case **real** (Čerenkov) photons are emitted, and the emission angle is called Čerenkov angle ϑ_c.

N.B. In discontinuous media diffraction causes real photon emission even if (3) is not fulfilled (transition radiation).

Cross-section for emission (see Appendix for details)

$$\frac{d\sigma}{d(\hbar\omega)} = \frac{\alpha}{\beta^2 \pi} \frac{\sigma_\gamma(\hbar\omega)}{\hbar\omega Z} \log \left[(1 - \beta^2 \epsilon_1)^2 + \beta^4 \epsilon_2^2\right]^{-\frac{1}{2}}$$

$$+ \frac{\alpha}{\beta^2 \pi} \frac{\sigma_\gamma(\hbar\omega)}{\hbar\omega Z} \log \left[\frac{2mc^2\beta^2}{\hbar\omega}\right] \qquad \text{(ionis., excit.} \to \text{dE/dx)}$$

$$+ \frac{\alpha}{\beta^2 \pi} \frac{1}{n_e \hbar c} \left[\beta^2 - \frac{\epsilon_1}{|\epsilon|^2}\right]\Theta \qquad \text{(Čerenkov, TRD)}$$

$$+ \frac{\alpha}{\beta^2 \pi} \frac{1}{(\hbar\omega)^2} \int_0^{\hbar\omega} \frac{\sigma_\gamma(\hbar\omega')}{Z} d(\hbar\omega') \qquad (\delta \text{ electrons)}$$

Basics: dE/dx, Čerenkov, Trans. Rad – 3

Related to $1/\varepsilon_2$

$\varepsilon_1 - 1$
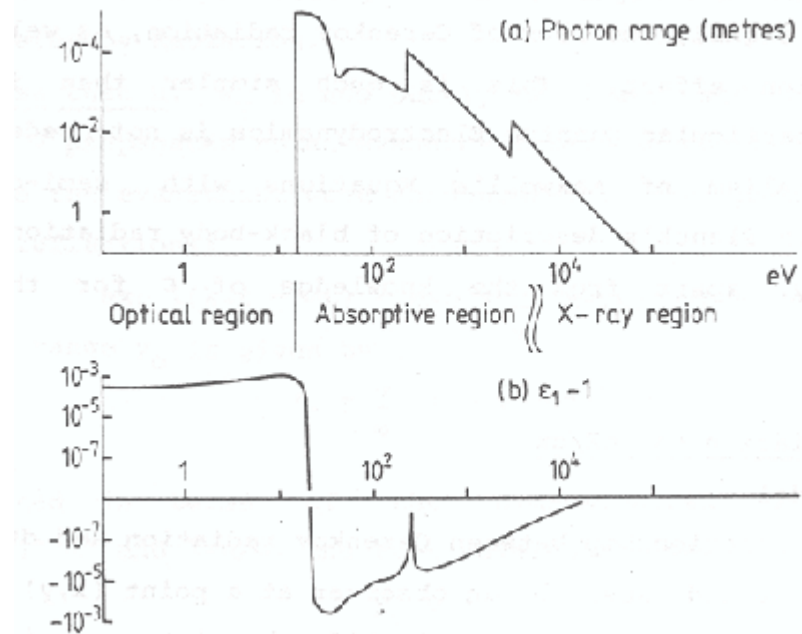
Three frequency ranges: ε_1, ε_2 vs frequency

1) Optical region: ε real and >1. The medium is transparent. and Čerenkov radiation is emitted by particles with velocity above the threshold.

2) Absorptive region: ε complex. Imaginary part makes the range of photons short.

3) X-ray region: ε nearly real and <1. Čerenkov threshold is greater than c, but sub-threshold Čerenkov radiation can be emitted at discontinuities in the medium --> X-ray Transition Radiation.

Derivation of dσ/d(hω) a la Allison, Cobb

- Solve Maxwell's Equations with charge density
  $\rho = e_0 \delta^3(\vec{r} - \vec{\beta}ct)$ and current density $\vec{j} = \vec{\beta}c\rho \rightarrow$
  $$\phi(\vec{k}, \omega) = \frac{e_0}{2\pi\epsilon\epsilon_0 k^2}\delta(\omega - \vec{k} \cdot \vec{\beta}c)$$
  $$\vec{A}(\vec{k}, \omega) = \frac{e_0}{2\pi\epsilon_0 c^2}\frac{(\omega\vec{k}/k^2 - \vec{\beta}c)}{(\epsilon\omega^2/c^2 - k^2)}\delta(\omega - \vec{k} \cdot \vec{\beta}c)$$
  $$\rightarrow \vec{E}(\vec{r}, t) =$$
  $$\frac{1}{(2\pi)^2}\int\int\left[i\omega\vec{A}(\vec{k}, \omega) - i\vec{k}\phi(\vec{k}, \omega)\right]e^{i(\vec{k}\cdot\vec{r} - \omega t)}d^3k\, d\omega \quad \text{(A1)}$$

- The energy loss is due to the component of this electric field in the direction β doing work on the particle at the point $\vec{r} = \vec{\beta}ct$:
  $$< \frac{dE}{dx} > = \frac{e_0}{\beta}\vec{E}(\vec{\beta}ct, t) \cdot \vec{\beta} \quad \text{(A2)}$$

- The energy loss is re-written as a probability of energy transfers
  $$< \frac{dE}{dx} > =$$
  $$-\int_0^\infty d(\hbar\omega)\int_{\frac{\hbar\omega}{\beta c}}^\infty d(\hbar k)\ n_e\hbar\omega\frac{d^2\sigma}{d(\hbar\omega)d(\hbar k)} \quad \text{(A3)}$$

  where n_e is the electron density and $\frac{d^2\sigma}{d(\hbar\omega)d(\hbar k)}$ is the double differential cross section per electron.

Derivation of dσ/d(hω) a la Allison, Cobb - 2

Comparing (A1) and (A2) with (A3) we derive

$$\frac{d^2\sigma}{d(\hbar\omega)d(\hbar k)} =$$

$$\frac{e_0^2}{4\pi\epsilon_0}\frac{2}{n_e\pi\hbar^2\beta^2}\left[p(\beta^2 - \frac{E^2}{p^2c^2})m\frac{1}{(\epsilon E^2 - p^2c^2)} - \frac{1}{pc^2}m\frac{1}{\epsilon}\right]$$

This formula already shows the $1/\beta^2$ factor which dominates the rate of energy loss at non relativistic velocities.

– Determine the complex function $\epsilon(k,\omega) = \epsilon_1 + i\epsilon_2$
  - photoabsorption from cross-section $\sigma_\gamma(\hbar\omega)$ and sum rules $\rightarrow \epsilon_2$ for on mass-shell photons ($\omega = kc$),
  - the Kramers-Kronig relation $\rightarrow \epsilon_1$ in terms of ϵ_2,
  - the dipole approximation $\rightarrow$ for small k $\epsilon(k,\omega)$ is independent of k at fixed ω,
  - constituent scattering from quasi-free electrons and the Bethe sum rule $\rightarrow \epsilon$ in the large k off-mass-shell region.

– Integrate the cross section over momentum transfer

$$\frac{d\sigma}{d(\hbar\omega)} = \frac{\alpha}{\beta^2\pi}\frac{\sigma_\gamma(\hbar\omega)}{\hbar\omega Z}\log\left[(1 - \beta^2\epsilon_1)^2 + \beta^4\epsilon_2^2\right]^{-\frac{1}{2}}$$

$$+ \frac{\alpha}{\beta^2\pi}\frac{\sigma_\gamma(\hbar\omega)}{\hbar\omega Z}\log\left[\frac{2mc^2\beta^2}{\hbar\omega}\right]$$

$$+ \frac{\alpha}{\beta^2\pi}\frac{1}{n_e\hbar c}\left[\beta^2 - \frac{\epsilon_1}{|\epsilon|^2}\right]\Theta$$

$$+ \frac{\alpha}{\beta^2\pi}\frac{1}{(\hbar\omega)^2}\int_0^{\hbar\omega}\frac{\sigma_\gamma(\hbar\omega')}{Z}d(\hbar\omega')$$

where $\alpha = \frac{e^2}{4\pi\epsilon_0\hbar c}$ is the fine structure constant, ϵ_1 and ϵ_2 are the real and imaginary parts of the on-mass-shell dielectric constant and

Mean excitation energy vs Z
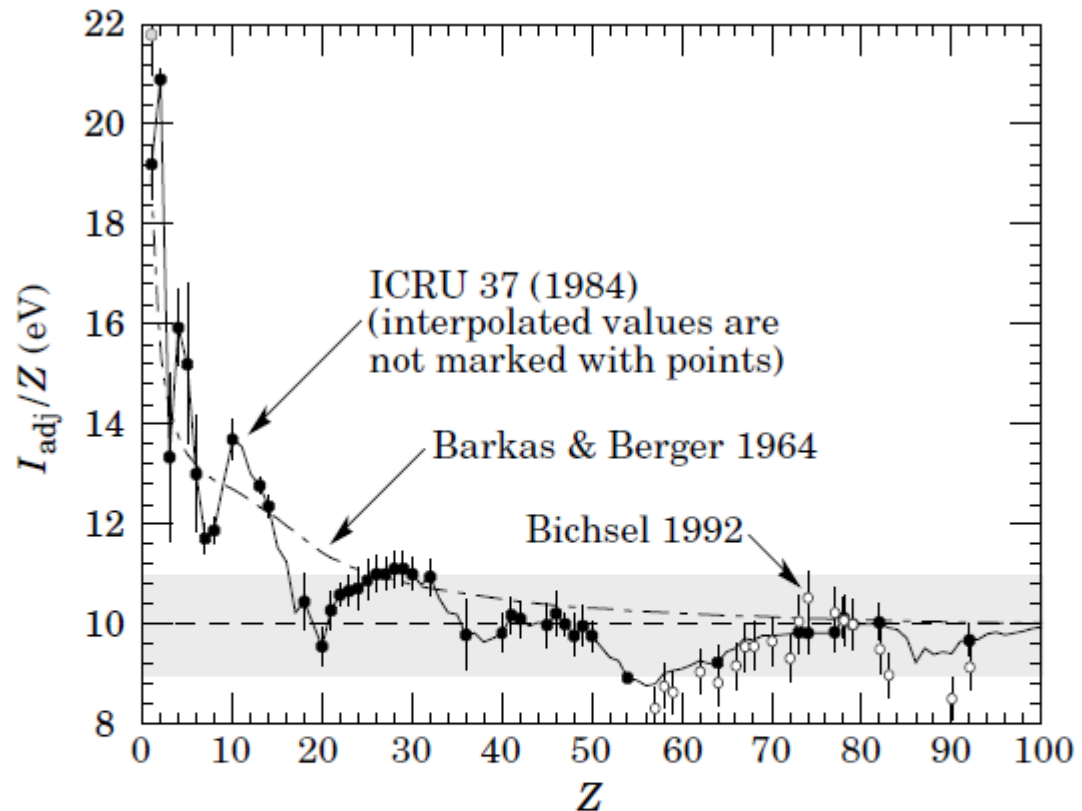
Figure 27.5: Mean excitation energies (divided by Z) as adopted by the ICRU [8]. Those based on experimental measurements are shown by symbols with error flags; the interpolated values are simply joined. The grey point is for liquid H_2; the black point at 19.2 eV is for H_2 gas. The open circles show more recent determinations by Bichsel [10]. The dotted curve is from the approximate formula of Barkas [11] used in early editions of this *Review*.

Mean energy loss in different materials
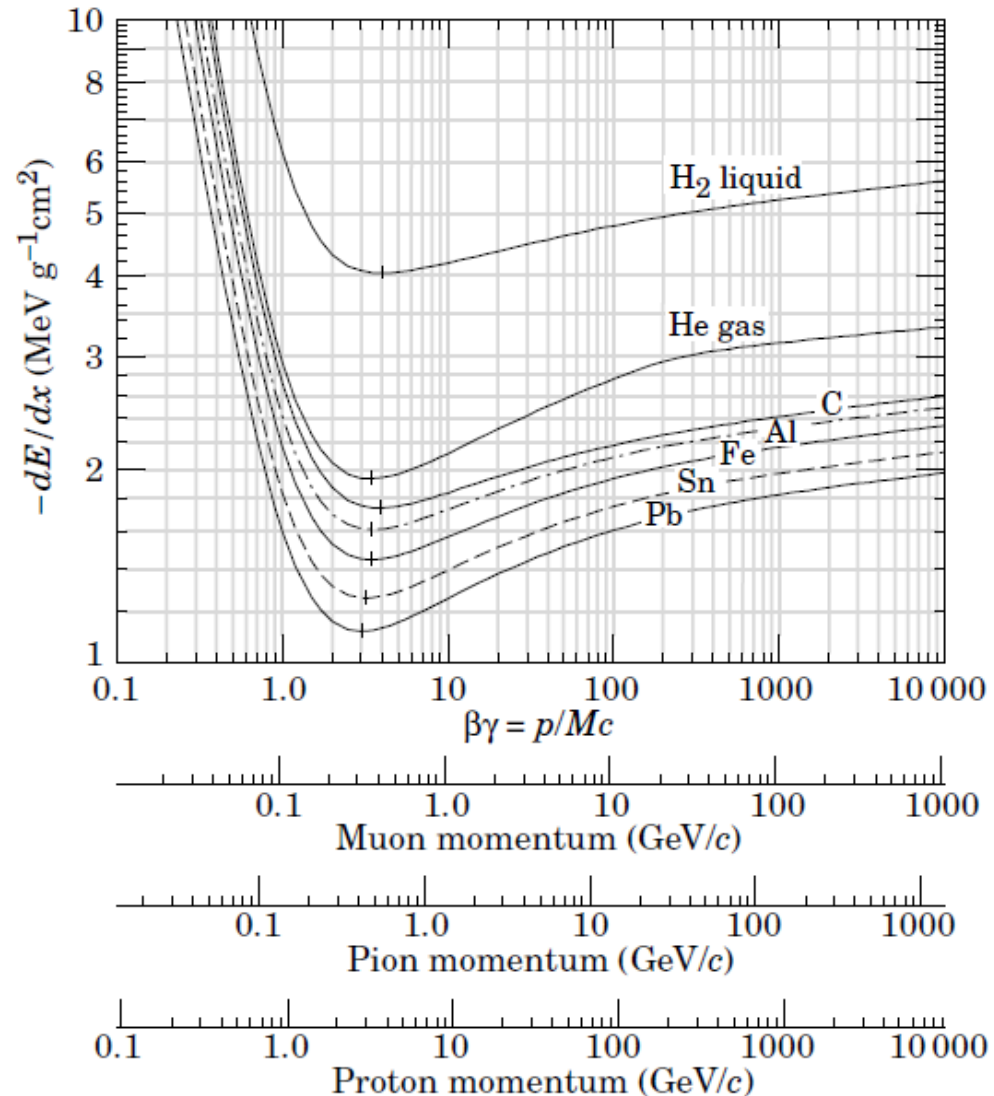
Figure 27.3: Mean energy loss rate in liquid (bubble chamber) hydrogen, gaseous helium, carbon, aluminum, iron, tin, and lead. Radiative effects, relevant for muons and pions, are not included. These become significant for muons in iron for $\beta\gamma \gtrsim 1000$, and at lower momenta for muons in higher-Z absorbers. See Fig. 27.21.

Energy loss at minimum for different materials

Figure 27.2: Stopping power at minimum ionization for the chemical elements. The straight line is fitted for $Z > 6$. A simple functional dependence on Z is not to be expected, since $\langle -dE/dx \rangle$ also depends on other variables.
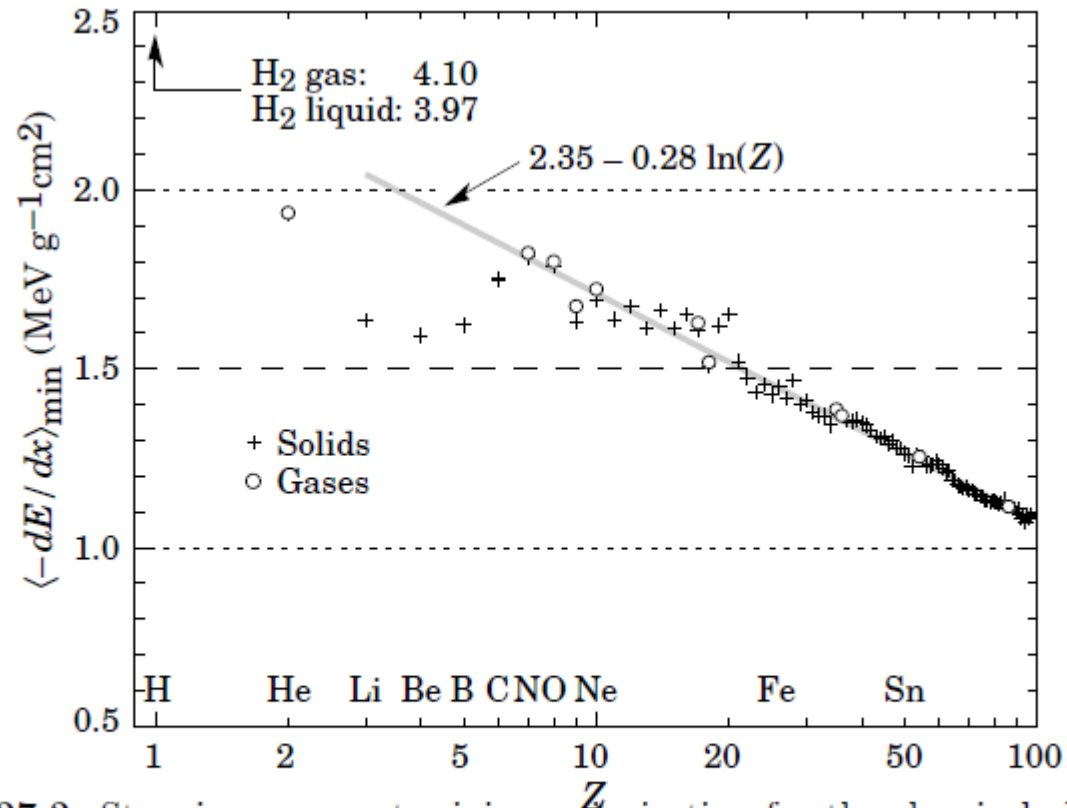
Energy loss as a function of energy of a heavy particle
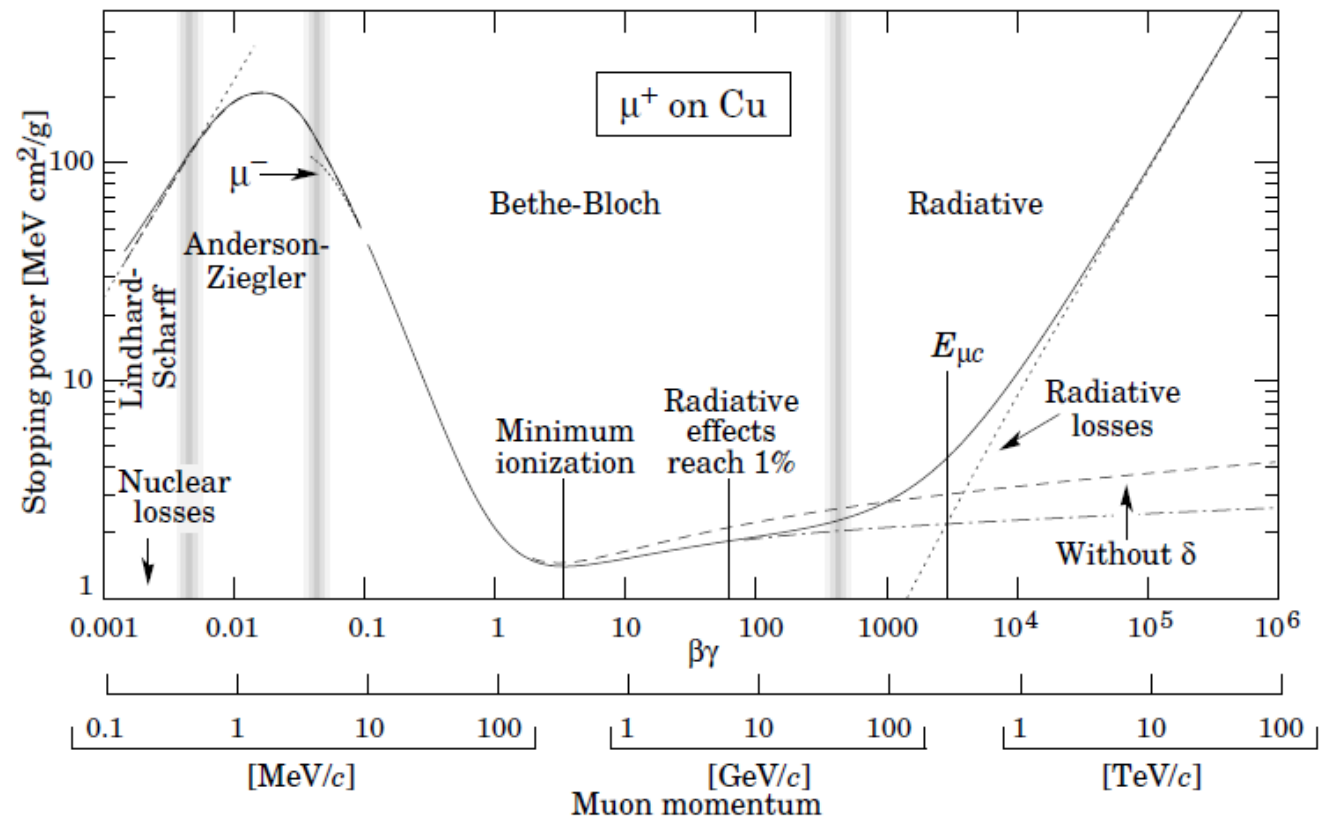
Fig. 27.1: Stopping power ($= \langle -dE/dx \rangle$) for positive muons in copper as a function of $\beta\gamma = p/Mc$ over nine orders of magnitude in momentum (12 orders of magnitude in kinetic energy). Solid curves indicate the total stopping power. Data below the break at $\beta\gamma \approx 0.1$ are taken from ICRU 49 [2], and data at higher energies are from Ref. 1. Vertical bands indicate boundaries between different approximations discussed in the text. The short dotted lines labeled "μ^-" illustrate the "Barkas effect," the dependence of stopping power on projectile charge at very low energies [3].

Stopping of heavy charged particles in matter: energy loss and range
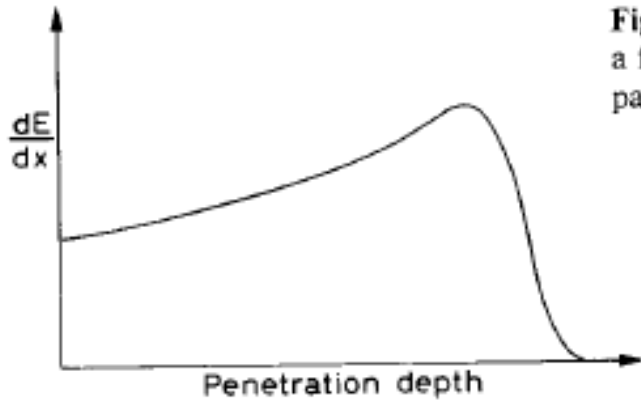
Fig. 2.5. A typical Bragg curve showing the variation of dE/dx as a function of the penetration depth of the particle in matter. The particle is more ionizing towards the end of its path

energy loss vs path length
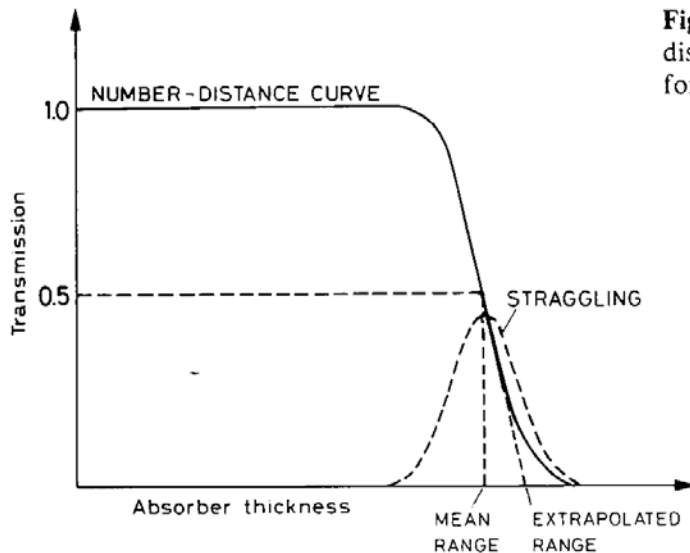
Fig. 2.7. Typical range number-distance curve. The distribution of ranges is approximately Gaussian in form

Transmission vs material thickness

Range
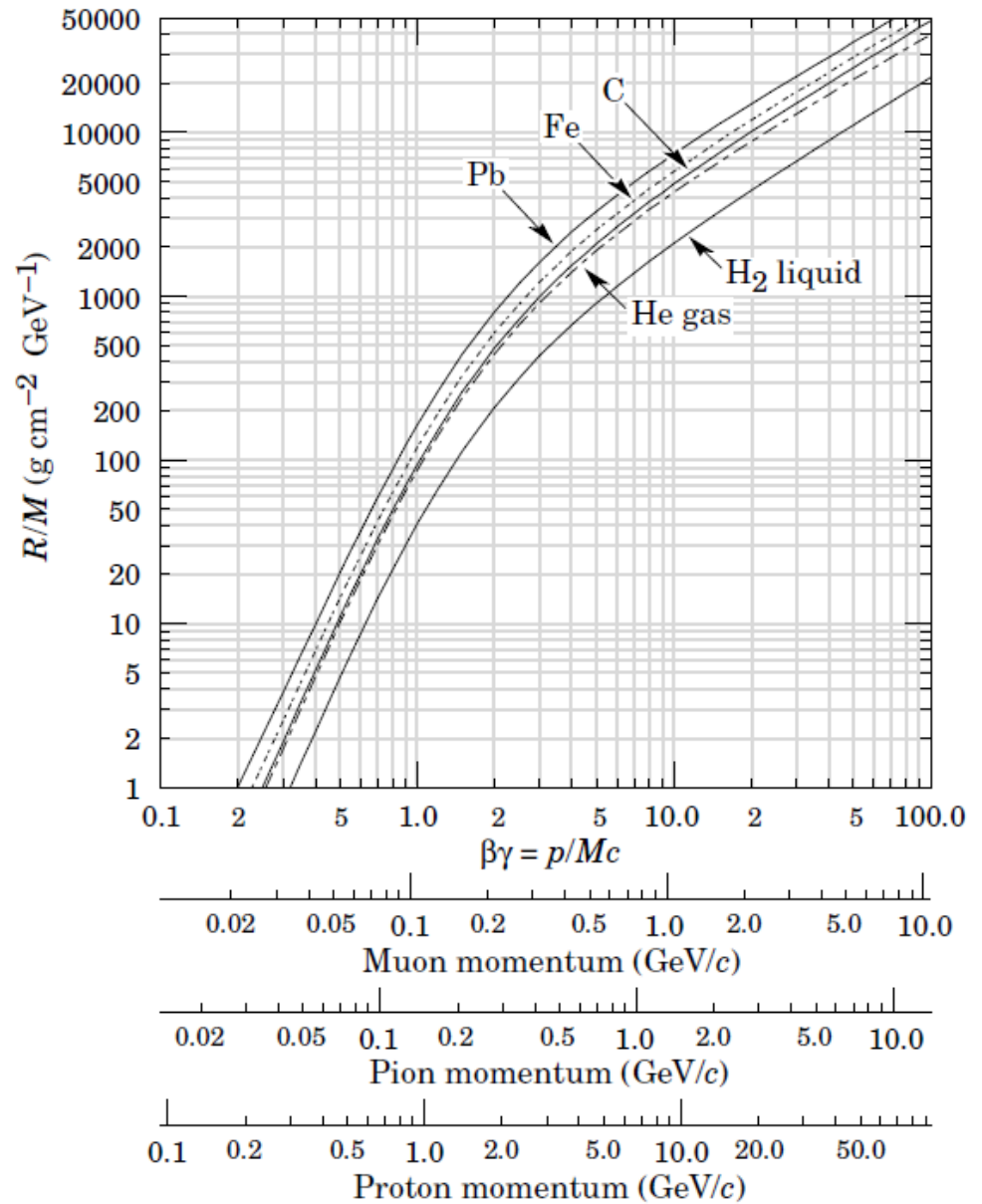
Figure 27.4: Range of heavy charged particles in liquid (bubble chamber hydrogen, helium gas, carbon, iron, and lead. For example: For a K^+ who momentum is 700 MeV/c, $\beta\gamma = 1.42$. For lead we read $R/M \approx 396$, and so range is 195 g cm^{-2}.

Straggling functions: energy loss distribution
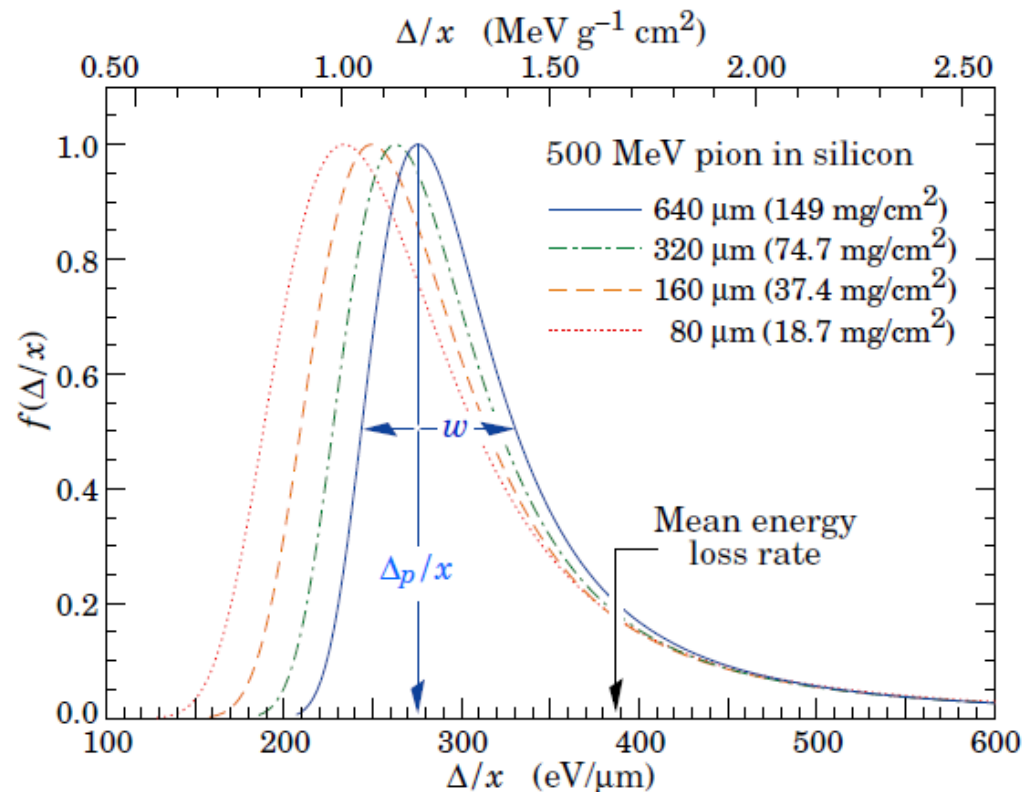
Figure 27.7: Straggling functions in silicon for 500 MeV pions, normalized to unity at the most probable value δ_p/x. The width w is the full width at half maximum. See full-color version on color pages at end of book.
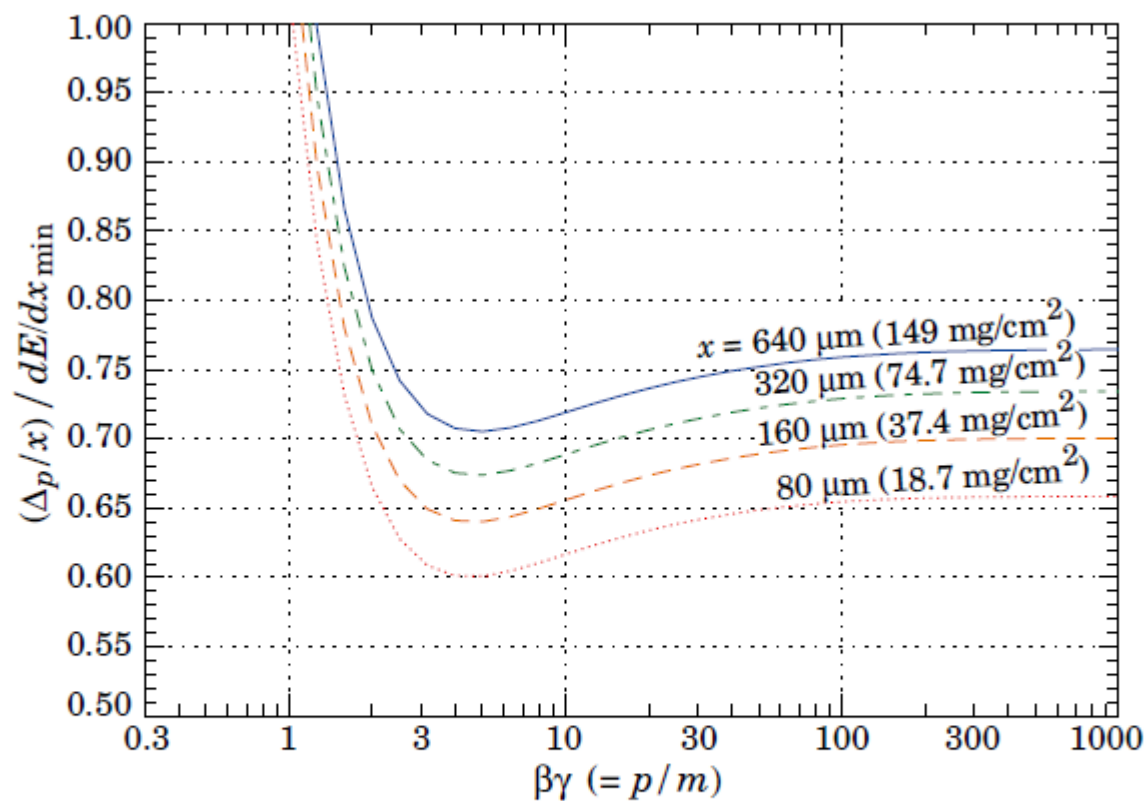
Figure 27.8: Most probable energy loss in silicon, scaled to the mean loss of a minimum ionizing particle, 388 eV/μm (1.66 MeV g^{-1}cm^2). See full-color version on color pages at end of book.

Energy loss distribution
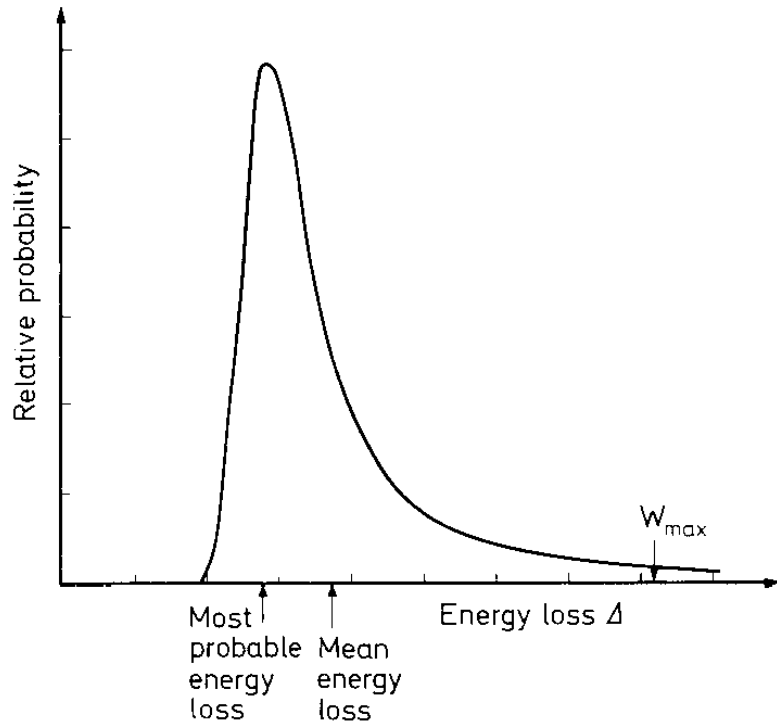
Fig. 2.18. Typical distribution of energy loss in a thin absorber. Note that it is asymmetric with a long high energy tail

Energy loss distribution
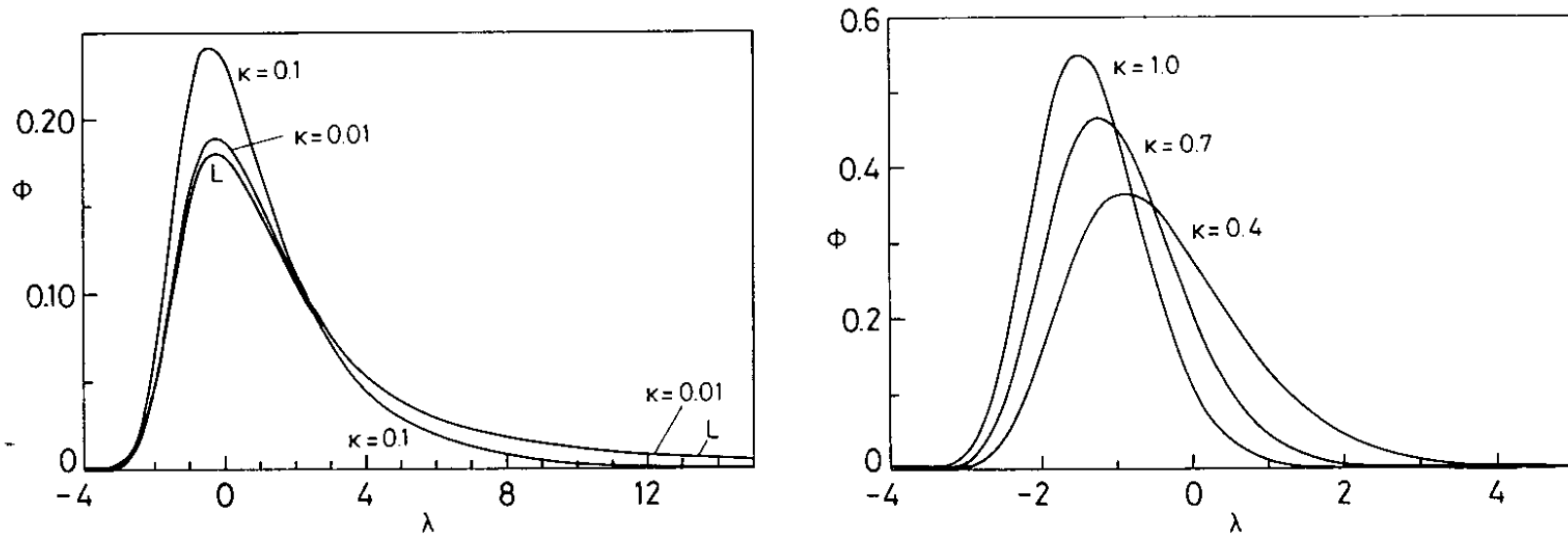
Fig. 2.19. Vavilov distributions for various κ. For comparison, Landau's distribution (denoted by the L) for $\kappa = 0$ is also shown (from *Seltzer* and *Berger* [2.29])

Energy loss distribution
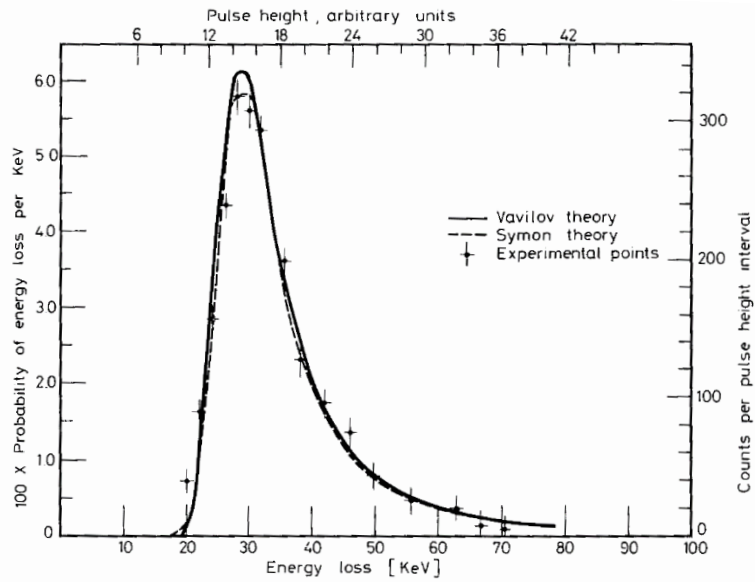
Fig. 2.20. Comparison of Vavilov's and Symon's theories with experiment (from *Seltzer* and *Berger* [2.29])

Multiple Coulomb scattering
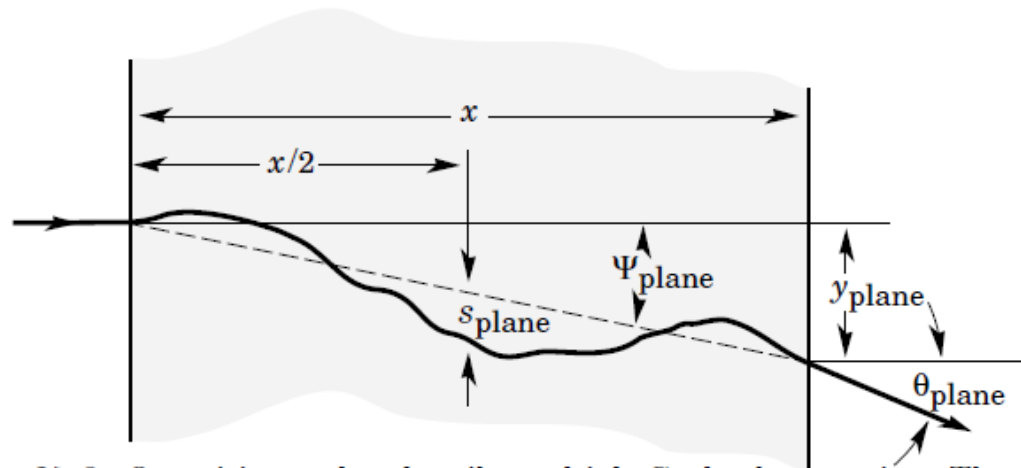
Figure 27.9: Quantities used to describe multiple Coulomb scattering. The particle is incident in the plane of the figure.

Electrons: fractional energy loss, 1/E dE/dx
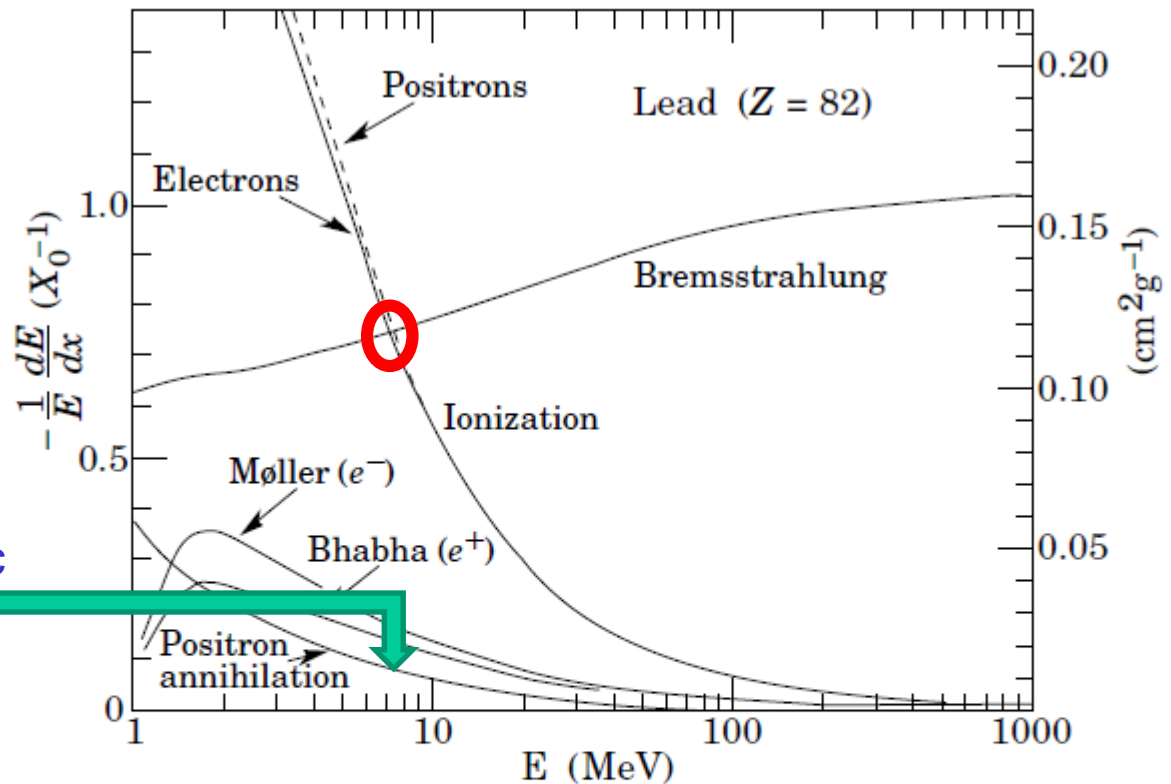
Figure 27.10: Fractional energy loss per radiation length in lead as a function of electron or positron energy. Electron (positron) scattering is considered as ionization when the energy loss per collision is below 0.255 MeV, and as Møller (Bhabha) scattering when it is above. Adapted from Fig. 3.2 from Messel and Crawford, *Electron-Photon Shower Distribution Function Tables for Lead, Copper, and Air Absorbers*, Pergamon Press, 1970. Messel and Crawford use $X_0(\text{Pb}) = 5.82$ g/cm^2, but we have modified the figures to reflect the value given in the Table of Atomic and Nuclear Properties of Materials ($X_0(\text{Pb}) = 6.37$ g/cm^2).

Critical energy E_c

# Very high energy muons: bremsstrahlung like electrons
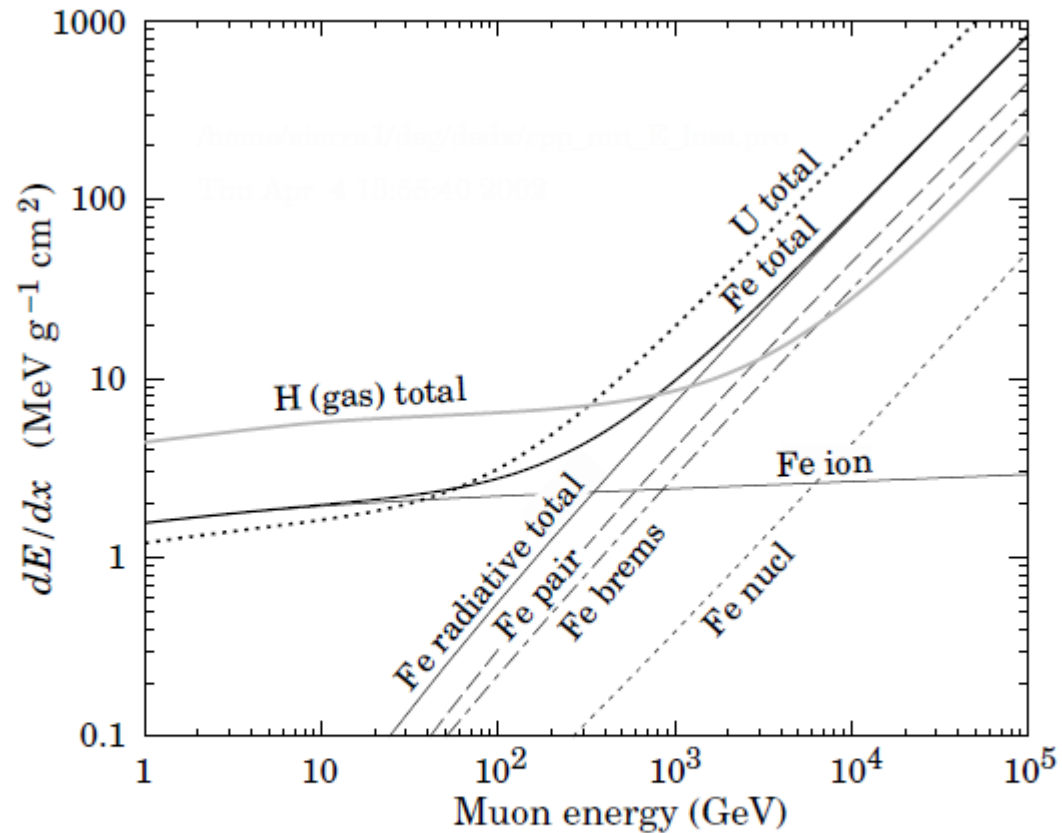
Figure 27.21: The average energy loss of a muon in hydrogen, iron, and uranium as a function of muon energy. Contributions to dE/dx in iron from ionization and the processes shown in Fig. 27.20 are also shown.

Stopping of electrons in matter

Absorption of homogeneous β-rays in aluminium

Transmission vs material thickness
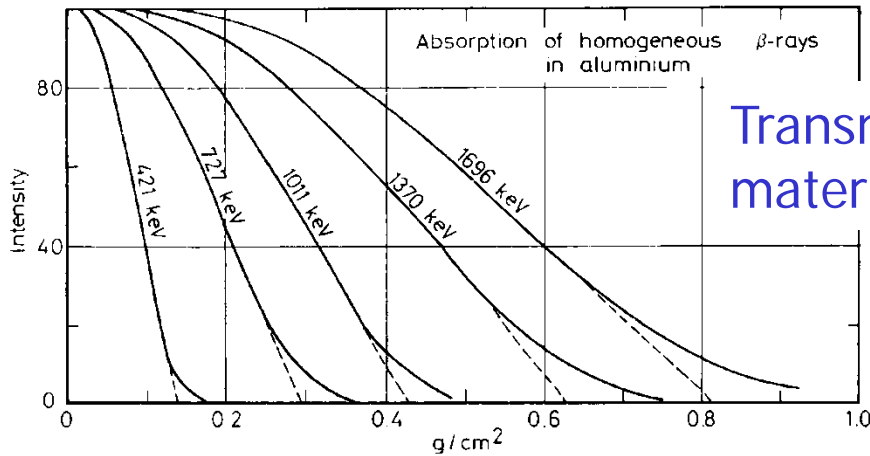
◄ **Fig. 2.11.** Range number-distance curves for electro (from *Marshall* and *Ward* [2.15])

Fig. 2.12. Range curves for electrons in several materials calculated in the continuous slowing down approximati (data from [2.16])

**Fig. 2.13.** Absorption curves for beta decay electrons fro ^{185}W (from *Baltakamens* et al. [2.17])

**Range for electrons**
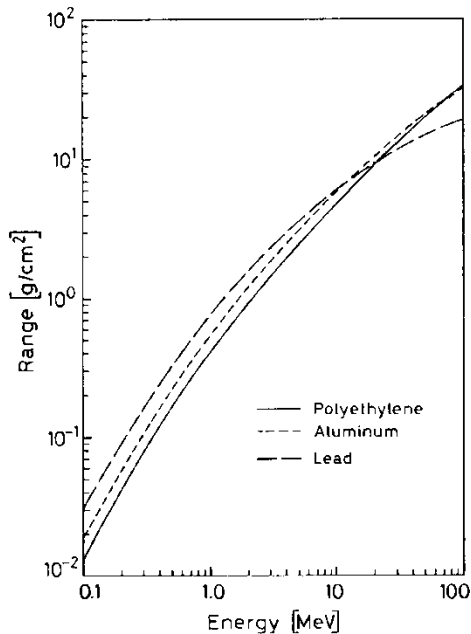
Fig. 2.12
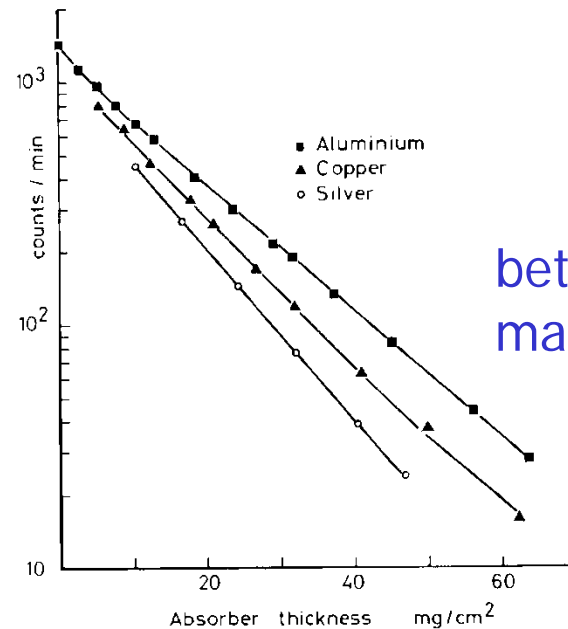
beta electrons vs material thickness

Fig. 2.13

Low energy electron scattering off a thin foil
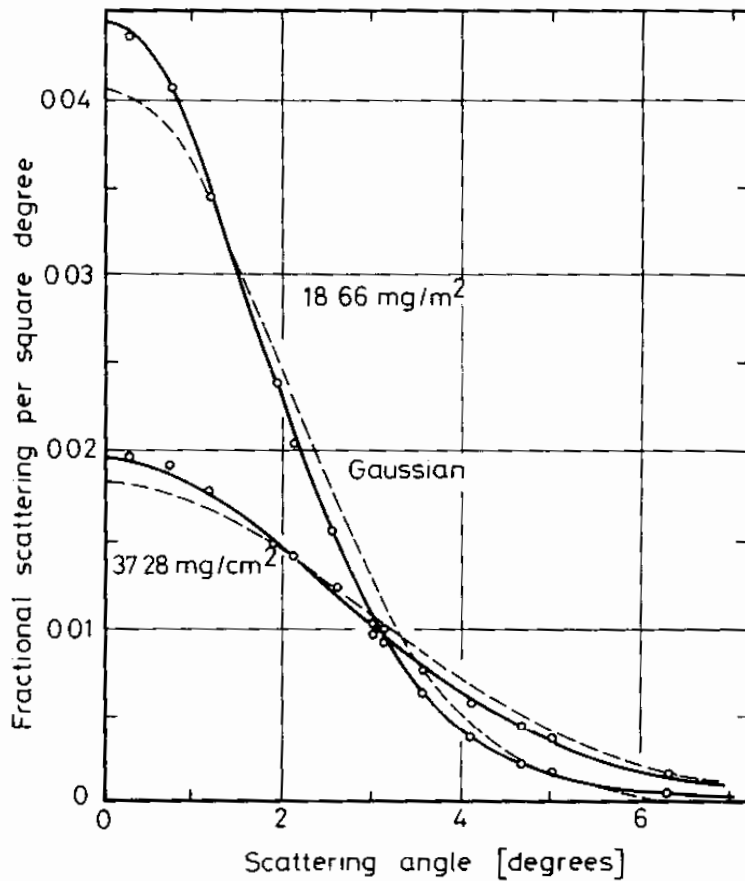
Fig. 2.15. Angular distribution of 15.7 MeV electrons scattered from a thin Au foil (from *Hanson* et al. [2.22]). The experimental values are compared with the Gaussian approximation to multiple scattering

Low energy electron back-scattering
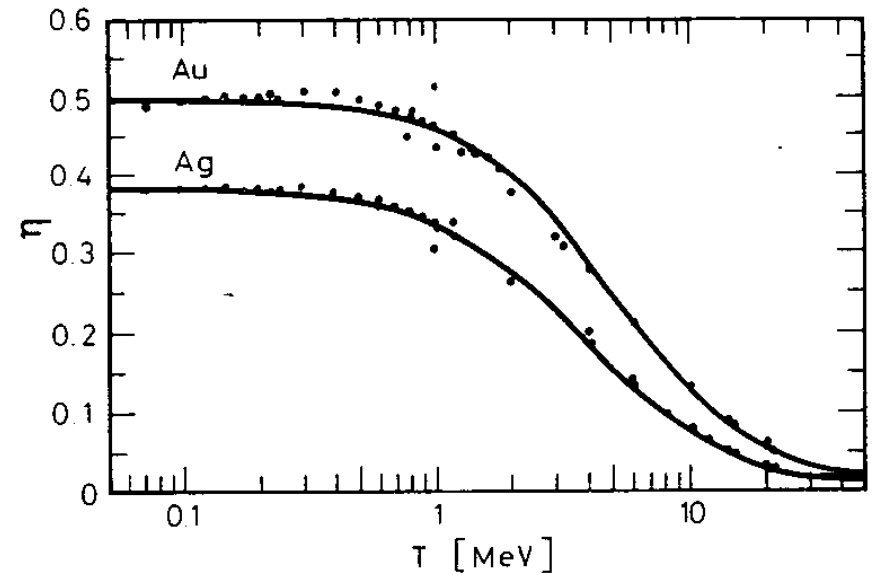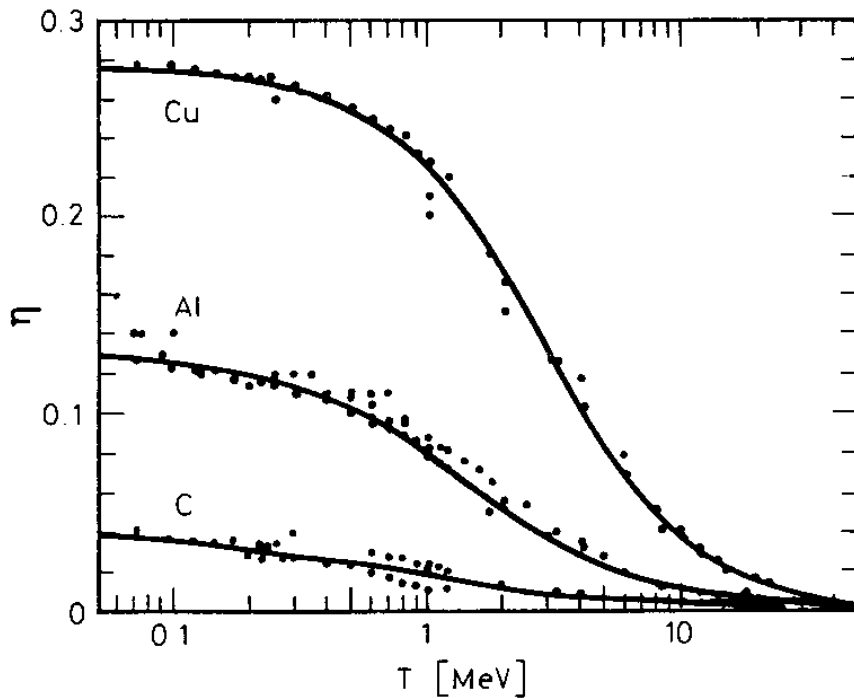
Fig. 2.17. Some measured electron backscattering coefficients for various materials. The electrons are perpendicularly incident on the surface of the sample (from *Tabata* et al. [2.24])

Interaction of photons with matter
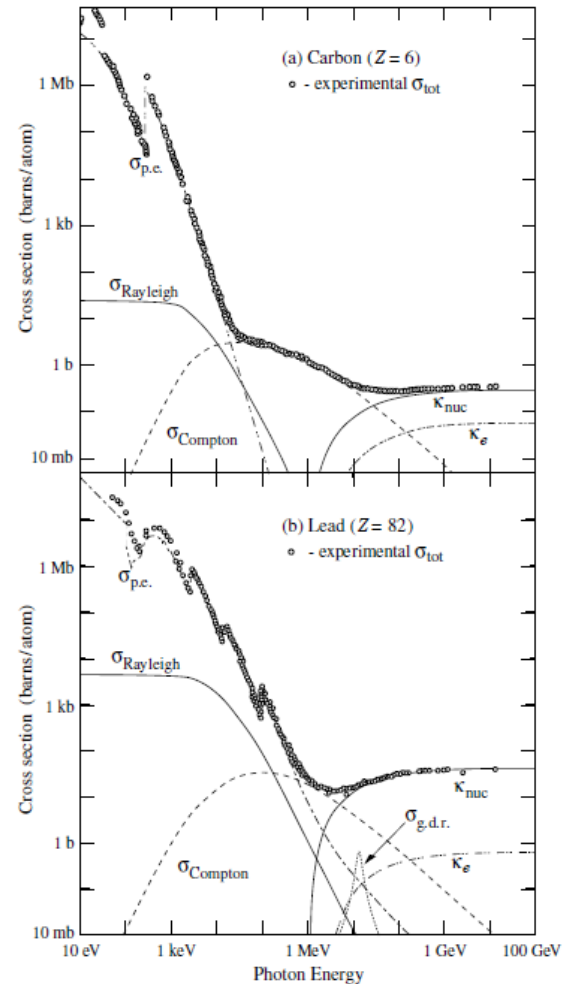
Figure 27.14: Photon total cross sections as a function of energy in carbon and lead, showing the contributions of different processes:

$\sigma_{p.e.}$ = Atomic photoelectric effect (electron ejection, photon absorption)

$\sigma_{Rayleigh}$ = Rayleigh (coherent) scattering–atom neither ionized nor excited

$\sigma_{Compton}$ = Incoherent scattering (Compton scattering off an electron)

κ_{nuc} = Pair production, nuclear field

κ_e = Pair production, electron field

$\sigma_{g.d.r.}$ = Photonuclear interactions, most notably the Giant Dipole Resonance [46]. In these interactions, the target nucleus is broken up.
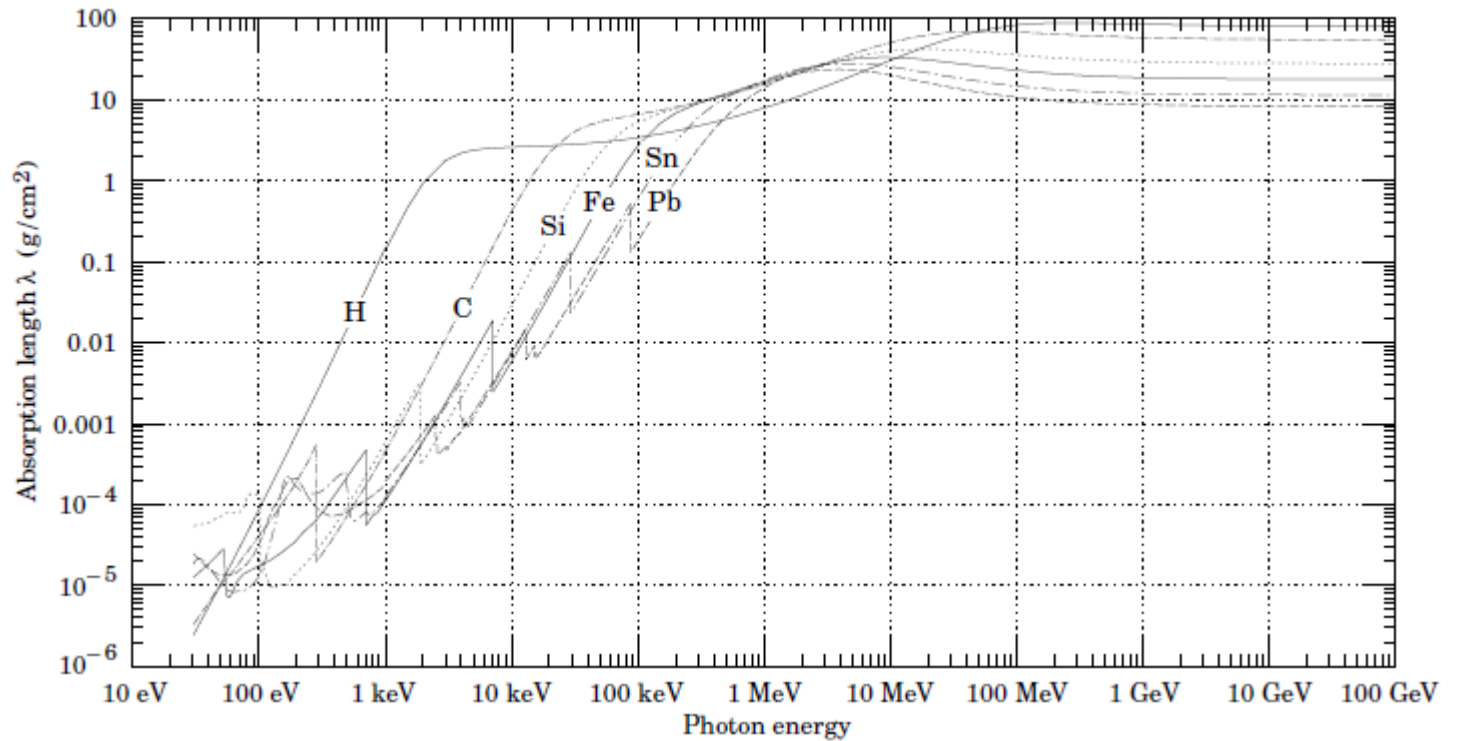
Figure 27.16: The photon mass attenuation length (or mean free path) $\lambda = 1/(\mu/\rho)$ for various elemental absorbers as a function of photon energy. The mass attenuation coefficient is μ/ρ, where ρ is the density. The intensity I remaining after traversal of thickness t (in mass/unit area) is given by $I = I_0 \exp(-t/\lambda)$. The accuracy is a few percent. For a chemical compound or mixture, $1/\lambda_{\text{eff}} \approx \sum_{\text{elements}} w_Z/\lambda_Z$, where w_Z is the proportion by weight of the element with atomic number Z. The processes responsible for attenuation are given in not Fig. 27.10. Since coherent processes are included, not all these processes result in energy deposition. The data for 30 eV $< E <$ 1 keV are obtained from `http://www-cxro.lbl.gov/optical_constants` (courtesy of Eric M. Gullikson, LBNL). The data for 1 keV $< E <$ 100 GeV are from `http://physics.nist.gov/PhysRefData`, through the courtesy of John H. Hubbell (NIST).
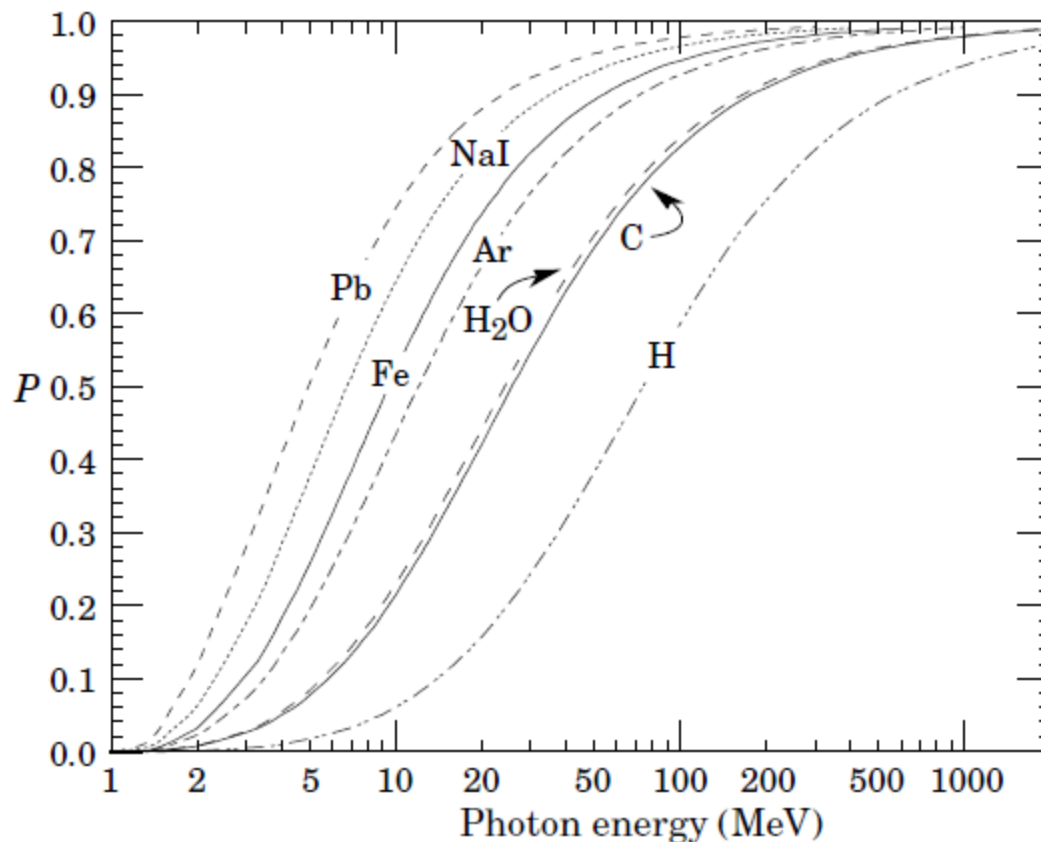
Figure 27.17: Probability P that a photon interaction will result in conversion to an e^+e^- pair. Except for a few-percent contribution from photonuclear absorption around 10 or 20 MeV, essentially all other interactions in this energy range result in Compton scattering off an atomic electron. For a photon attenuation length λ (Fig. 27.16), the probability that a given photon will produce an electron pair (without first Compton scattering) in thickness t of absorber is $P[1 - \exp(-t/\lambda)]$.
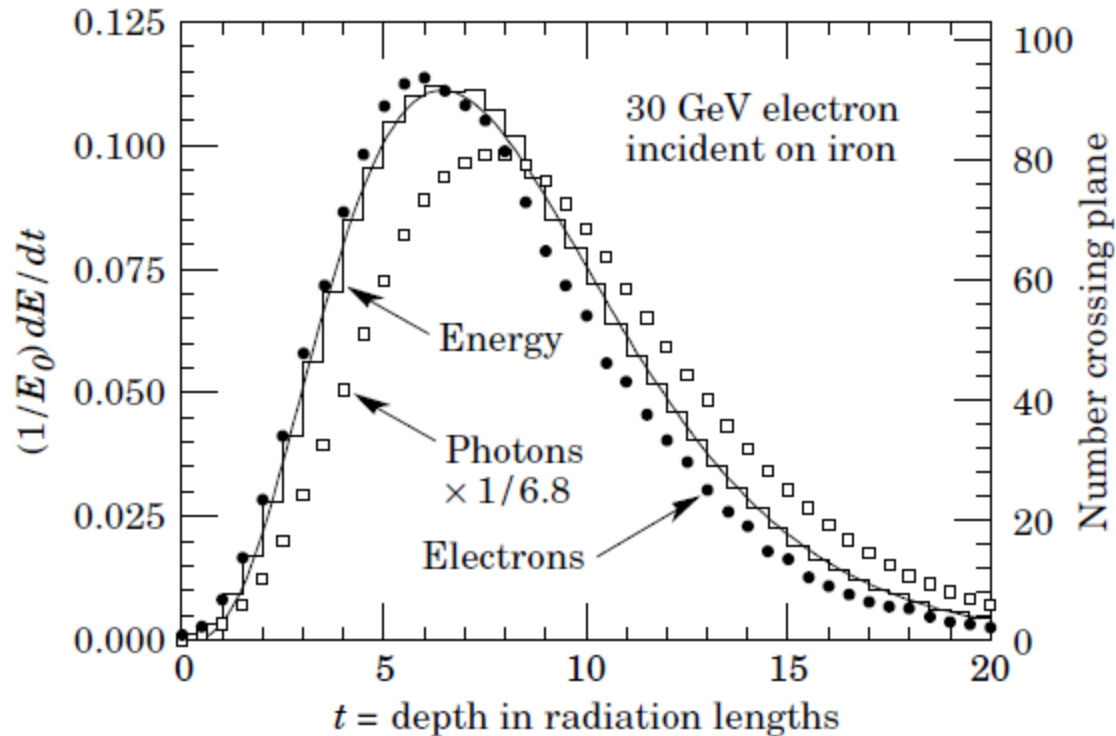
Figure 27.18: An EGS4 simulation of a 30 GeV electron-induced cascade in iron. The histogram shows fractional energy deposition per radiation length, and the curve is a gamma-function fit to the distribution. Circles indicate the number of electrons with total energy greater than 1.5 MeV crossing planes at $X_0/2$ intervals (scale on right) and the squares the number of photons with $E \geq 1.5$ MeV crossing the planes (scaled down to have same area as the electron distribution).

Photons: Compton scattering
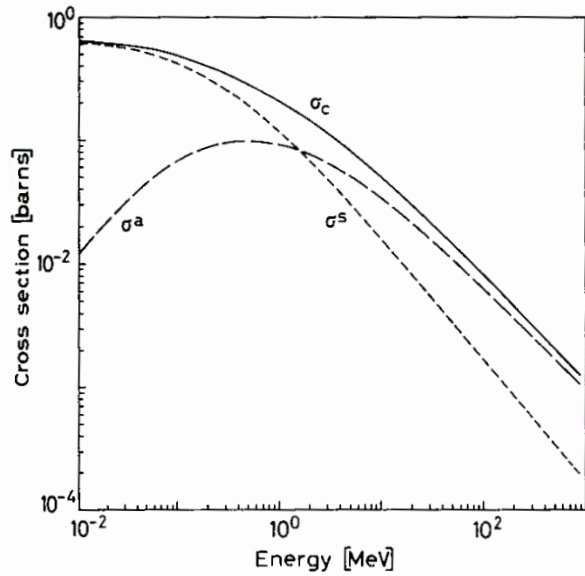
Compton scattering
cross section

Fig. 2.23. Total Compton scattering cross sections

Compton scattering:
electron energy
distribution
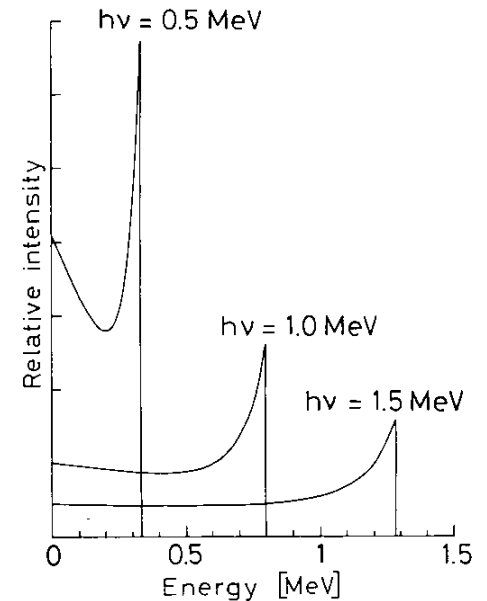
Fig. 2.24. Energy distribution of Compton recoil electrons. The sharp drop at the maximum recoil energy is known as the *Compton edge*

Photons: pair production

Pair production cross section in Pb
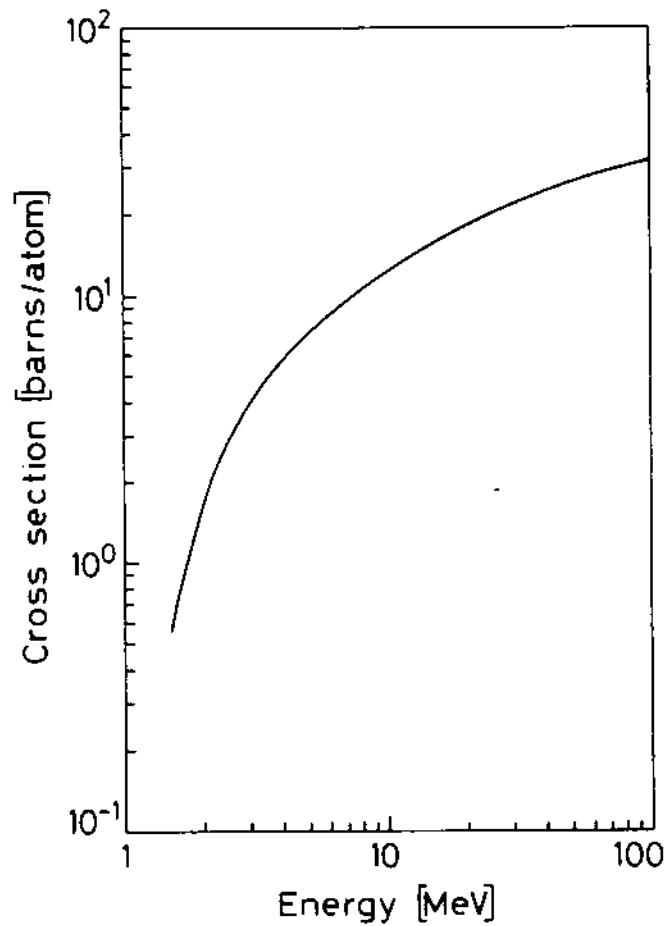
Fig. 2.25. Pair production cross section in lead